JACS
JOURNAL OF THE AMERICAN CHEMICAL SOCIETY

Communication

pubs.acs.org/JACS

Kinetics Tuning of Li-Ion Diffusion in Layered $Li(Ni_xMn_yCo_z)O_2$

Yi Wei,[†,#] Jiaxin Zheng,[†,#] Suihan Cui,[†,#] Xiaohe Song,[†] Yantao Su,[†] Wenjun Deng,[†] Zhongzhen Wu,[†] Xinwei Wang,[†] Weidong Wang,[‡] Mumin Rao,[§] Yuan Lin,[†] Chongmin Wang,[∥] Khalil Amine,[⊥] and Feng Pan*[,†]

[†]School of Advanced Materials, Peking University, Shenzhen Graduate School, Shenzhen 518055, People's Republic of China

[‡]Shenzhen Tianjiao Technology Development Co., Ltd., Shenzhen 518119, People's Republic of China

[§]Shenzhen OptimumNano Energy Co., Ltd., Shenzhen 518118, People's Republic of China

[∥]Environmental Molecular Science Laboratory, Pacific Northwest National Laboratory, 902 Battelle Boulevard, Richland, Washington 99352, United States

[⊥]Electrochemical Technology Program, Chemical Sciences and Engineering Division, Argonne National Laboratory, Argonne, Illinois 60439, United States

Supporting Information

ABSTRACT: Using ab initio calculations combined with experiments, we clarified how the kinetics of Li-ion diffusion can be tuned in $LiNi_xMn_yCo_zO_2$ (NMC, $x + y + z = 1$) materials. It is found that Li-ions tend to choose oxygen dumbbell hopping (ODH) at the early stage of charging (delithiation), and tetrahedral site hopping (TSH) begins to dominate when more than 1/3 Li-ions are extracted. In both ODH and TSH, the Li-ions surrounded by nickel (especially with low valence state) are more likely to diffuse with low activation energy and form an advantageous path. The Li slab space, which also contributes to the effective diffusion barriers, is found to be closely associated with the delithiation process (Ni oxidation) and the contents of Ni, Co, and Mn.

Rechargeable lithium-ion batteries (LIBs) not only power most of today's hybrid electric vehicles (HEV) and electric vehicles (EV)[1] but also are considered as a very promising system for renewable energy storage. For these newer applications, high power density is important, which is closely associated with the charge and discharge rate capability (CDR). The CDR is usually determined by the Li-ion and electron transport in the cathode materials.[2] As a result, fast Li-ion diffusivity in cathode materials is needed for high power density applications.

$LiNi_xMn_yCo_zO_2$ (NMC, $x + y + z = 1$) materials from solid-solution approaches to $LiMO_2$ (M = Ni, Mn, Co, etc.) without disturbing the layer structure have attracted much attention.[3] Compared with $LiCoO_2$, they not only possess high reversible capacity but also show better environmental compatibility and better Li-ion diffusivity.[4] Due to the charge redistribution, the oxidation state of transition metals in the NMC system (Ni^{2+}, Ni^{3+}, Co^{3+}, Mn^{4+}) is different from that in $LiMO_2$ (M = Ni^{3+}, Co^{3+}, Mn^{3+}). The three transition metals play different functions in the NMC system: the Ni participates in the redox behavior, acting as a double redox-active center with $Ni^{2+} \rightarrow Ni^{3+} \rightarrow Ni^{4+}$;[5] the Mn accounts for pushing some Ni atoms from Ni^{3+} to Ni^{2+} (introducing more reversible capacity) and some of the structure stability upon cycling;[6] the Co benefits a highly ordered and stable structure and is kept Co^{3+} before all Ni transformed to Ni^{4+} during charge and discharge.[7] Hereto, questions have been aroused: How do the functions of the three transition metals and their contents affect the Li-ion diffusivity in the layered NMC materials? How can the kinetics of Li-ion diffusion in layered NMC materials be tuned? Consequently, a detailed in-depth study is needed, which would share some clues to further optimize the transition metal contents to improve the Li-ion diffusivity in NMC materials.

Herein, using ab initio calculations combined with experiments, we investigate kinetic tuning of Li-ion diffusion in NMC materials systematically. Our calculations and experiments reveal that the kinetics of Li-ion diffusion in layered NMC can be tuned by the Li content (delithiation process) as well as the different contents of Ni, Co, and Mn. At the early stage of charging, Li-ions tend to choose oxygen dumbbell hopping, and tetrahedral site hopping begins to dominate when more than 1/3 Li-ions are extracted. The Li-ion diffusivity in the NMC system also depends on the content and valence state of Ni and the Li slab space, which are closely associated with the delithiation process (Ni oxidation) and the contents of Ni, Co, and Mn. The high content of Ni (especially for Ni^{2+}) is beneficial to the Li-ion diffusion, but appropriate contents of Mn and Co are also essential due to the correlated synergistic effect in the transition metal slab.

The studied NMC materials include $LiCoO_2$, $LiMnO_2$, $LiNiO_2$, and $LiNi_xMn_yCo_zO_2$ with (xyz) [Ni^{2+}:Ni^{3+}] = (333) [1:0], (442) [1:0], (552) [1:0], (550) [1:0], (532) [3:2], (622) [1:2], (71515) [3:11], and (811) [1:7].[4b,8] The minimum energy pathways and saddle points connecting Li-ion sites were calculated by the climbing-image nudged elastic band (cNEB) method,[9] and the diffusion coefficients for all NMC samples (Figure 1a) were calculated through the ab initio MD simulations. Figure 1b shows a representative supercell model for the (532) sample, which is also the most energy stable structure. The diffusion coefficient (D_s) is calculated as the averaged mean square displacement of Li atoms over time, and we obtain the D_s at rt (300 K) through an Arrhenius linear fitting

Received: April 24, 2015

DOI: 10.1021/jacs.5b04040
J. Am. Chem. Soc. XXXX, XXX, XXX−XXX

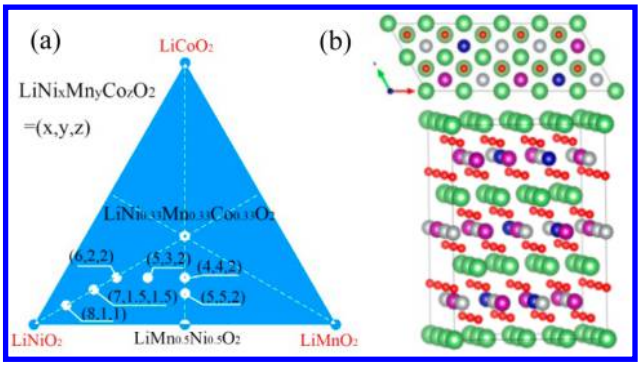

Figure 1. (a) The triangle shows the studied layered $LiNi_xMn_yCo_zO_2$ (NMC) ($x + y + z = 1$) cathode materials. (b) Top view and side view of the structure model for the multilattice of $LiNi_{0.5}Mn_{0.3}Co_{0.2}O_2$. Green, Li; red, O; silver, Ni; purple, Mn; blue, Co.

the D_s values at high temperatures (Figure S7). More details about the calculations can be found in the Supporting Information (SI). We also use the GITT method to measure the Li-ion diffusion coefficients of different NMC materials we prepared (SI) and compare the results with the calculated values.

First, the possible Li-ion diffusion pathways and their tuning factors in NMC materials were investigated. There are two kinds of Li diffusion pathways in such layered structures[10] (Figure 2).

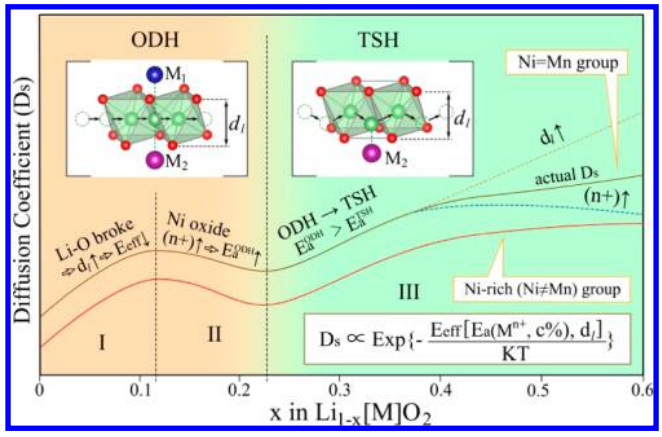

Figure 2. A global view of kinetics tuning of Li-diffusion in a delithiation process. E_{eff}: effective diffusion barrier as an index of NMC material's kinetic performance. Background colors (orange and green) illustrate the dominate area of TSH and ODH, respectively. The same Ni content is assumed for the "Ni = Mn" group and "Ni-rich" group.

One includes the Li-ions diffusing from one octahedral site to the next by hopping through the oxygen dumbbell directly, named oxygen dumbbell hopping (ODH). The activation barrier of ODH likely depends on the size of the saddle point of the oxygen dumbbell (strain effect) as well as the electrostatic interaction between the Li-ion in the activated state and the transition metal cations below and above it. Another involves Li-ions diffusing from one octahedral site to the next by hopping through a divacancy left by Li-diffusions to an intermediate tetrahedral site with a transition metal around, named tetrahedral site hopping (TSH). The size of the tetrahedral site (strain effect) as well as the electrostatic interaction between Li-ion in the activated state and the transition metal cation directly below it would contribute to the activation energy. As a result, the effective diffusion barriers (E_{eff}) in both ODH and TSH can be expressed as $E_{eff} = [E_a(M^{n+}, c\%), d_l]$, where M^{n+}, c%, $E_a(M^{n+}, c\%)$, and d_l denote the transition metal cations, the concentration of M^{n+}, activation energy of the electrostatic interaction contribution from the transition metal cations, and the Li slab space, respectively. It should be noted that TSH requires the presence of a divacancy, and the center Li-ion can diffuse from its original site to a nearby vacancy via TSH only when these Li vacancies stay together. The possibility for such a state is very small at the early stage of delithiation. For example, the TSH path is activated at state of charge (SOC) > 1/6, and the possibility of TSH is 2/5 at SOC = 1/3. By contrast, there is no such restriction for the ODH, and it should be the dominating Li-ion diffusion path at the early stage of charging.

The strain effect has already been studied by Kang et al. in $LiCoO_2$ and $LiNi_{0.5}Mn_{0.5}O_2$ for the TSH route.[2,11] They find that the activation barriers reduce with the increasing Li slab space linearly (e.g., the activation barrier for Ni^{2+} is reduced by a value of 0.1 eV when the Li slab space is increased by 0.1 Å.), indicating the sensitive relationship between the activation barrier and the Li slab space. Here we mainly studied the effect of the kind of transition metals and their valence states (Ni^{2+}, Ni^{3+}, Co^{3+}, and Mn^{4+}). The barriers in ODH in $Li(Ni_xCo_yMn_z)O_2$ depend on the two transition metal cations nearby. Figure 3 shows the

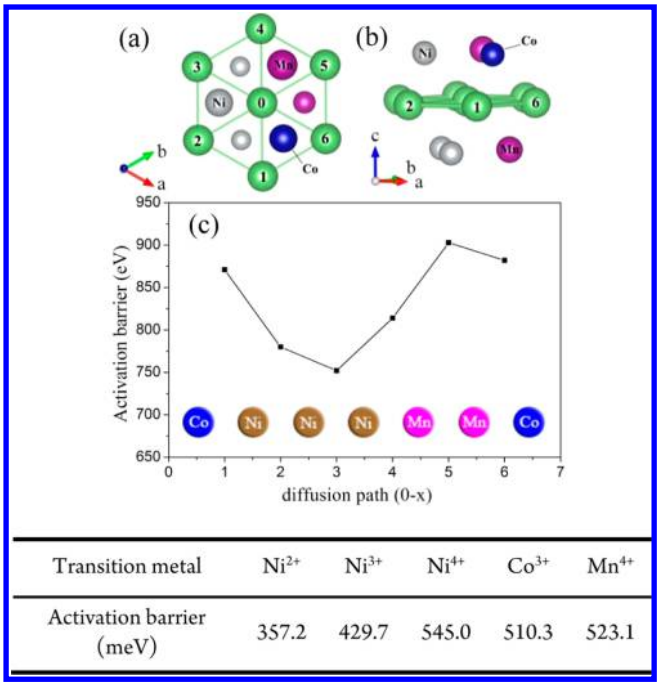

Transition metal	Ni^{2+}	Ni^{3+}	Ni^{4+}	Co^{3+}	Mn^{4+}
Activation barrier (meV)	357.2	429.7	545.0	510.3	523.1

Figure 3. (a and b) A view of the six ODH paths in the NMC crystal structure along and perpendicular to the c axis, respectively. (c) The activation energies from site 0 to sites 1−6 between two transition metal atoms. The table shows the activation energies for Li-ion TSH migration paths near different transition metal cations.

probable ODH paths and the corresponding diffusion barriers. Clearly, a low mixed valence transition metal such as Ni^{2+}/Ni^{3+} is beneficial to the Li diffusion, and the barrier for ODH near Ni^{3+}/Ni^{4+} is the second lowest. For TSH pathways, the energy barrier with 0.357 eV near the Ni^{2+} site is the lowest (table in Figure 3), indicating the fastest Li-ion diffusion, consistent with the results in ref 2. TSH near Ni^{3+} shows a higher diffusion barrier with 0.43 eV, but this value is still smaller than those near Co^{3+} and Mn^{4+}. It should be noticed that all the barriers of ODH are about two times higher than those in TSH, indicating that TSH is an energy favorable diffusion path once the divacancy exists. However, no matter which way is the dominating diffusion path, compared to

DOI: 10.1021/jacs.5b04040
J. Am. Chem. Soc. XXXX, XXX, XXX−XXX

Co^{3+} and Mn^{4+}, Ni^{2+} and Ni^{3+} always facilitate the Li-ion diffusion. As the delithiation process goes on from the fully Li-filled stage, advantageous paths along the sites with Ni (especially Ni^{2+}) were formed, in which the Li-ion would diffuse easily. When SOC reaches near 1/3 and TSH becomes the main mechanism of Li-ion hopping, Li-ions near these existing diffusion paths can easily find divacancies.

Combining the measured and calculated Li-ion diffusion coefficients under different SOCs for some representative NMC materials (Figure S8), we propose how those factors tune the kinetics of Li-ion diffusion in a delithiation process (Figure 2). Interestingly, the diffusion coefficients of all materials show the same trend with the Li content and a lowest value near SOC = 0.22−0.25. Previous experimental results also exhibit the same phenomenon, but miss giving the reason.[3c] Here the mechanism can be proposed that, during the early stage of delithiation, the Li slab space expands due to the removal of O^{2-}−Li^{+}−O^{2-} bonds across the slab to facilitate faster Li diffusion,[2] thus leading to the reduced E_{eff} and increased D_s (Figure 2, I). Meanwhile, the valence of nickel would rise from Ni^{2+} to Ni^{3+} and Ni^{4+} as the delithiation increased, and both ODH and TSH show an increased activation energy with the oxidation of nickel ions. This effect would become more dominant with the increasing delithiation and lead to the increased E_{eff} and decreased D_s (Figure 2, II). Based on previous discussions, when SOC exceeds 1/6, TSH arises and becomes the main hopping pathway when the SOC reaches 1/3. As a result, the tuning of Li-ion's hopping mechanism decreases the E_{eff} ($E_{eff}^{ODH} > E_{eff}^{TSH}$), and this effect would surpass the effect of the activation energy increased by Ni oxidation, thus resulting in the increased D_s when the SOC exceeds the point of minimum D_s value (SOC = 0.22−0.25) (Figure 2, III). Finally, after the TSH dominates the Li hopping mechanism, the competition between the increasing Li slab space and the increased Ni valence state during the delithiation (two dashed lines in Figure 2) comprises the slower increase for D_s (Figure 2).

Furthermore, we studied how the different contents of Ni, Co, and Mn, their valence states, and related concentrations in NMC materials tune the kinetics of Li-ion diffusion at the same SOC. According to the initial valence state of Ni, we divide the studied NMC materials into two groups: one group includes (532), (622), (71515), and (811), which can be considered as $LiNiO_2$ substituted solid solutions and named as Ni-rich group, and the Ni ions show mixed valence states of Ni^{2+}/Ni^{3+}. Another group includes (333), (442), (552), and (550), which is named the "Ni = Mn" group, and all the Ni ions show the Ni^{2+} state. Figure 4 shows a plot for all the calculated and measured diffusion coefficients (SOC = 1/3 and 1/2) at rt with the Ni content in the NMC system. Though there is a difference of nearly 2 orders of magnitude between the calculation values and experimental results, they show the same trend with increasing Ni content.

For the "Ni = Mn" group, the Li slab spaces are nearly the same for all of them so that the strain effect can be neglected here (Table S3). According to the former calculated activation barriers (E_a) for different transition metal cations, a high concentration of cations such as Ni^{2+} and Ni^{3+} would facilitate the Li-ion diffusion. When SOC = 1/3, the Ni^{2+} content increases with increasing Ni content along the "Ni = Mn" route, so the D_s increases with the Ni content (Figure 4). When at SOC = 1/2, though there is no Ni^{2+}, the Ni^{3+} content increases with the increasing Ni content, so the D_s also increases with the Ni content. The dramatic drop of D_s from (550) to (532) can be attributed to the much higher Ni^{2+} (Ni^{3+}) content in (550) at

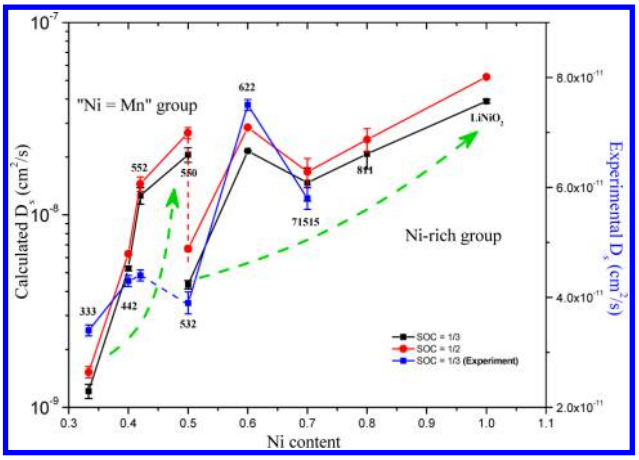

Figure 4. Calculated and experimental measured diffusion coefficient (D_s) of different NMC materials with nickel content in ascending order from left to right. D_s in both SOC = 1/2 and 1/3 are presented here with red and black points. The error bar for the calculated Ds corresponds to statistical uncertainty in the fitting of the mean square displacement to time curve.

SOC = 1/3 (SOC = 1/2) (Table S2). The reason why the D_s of (532) is even smaller than that of (552) at the same SOC is also similar. Figure S9 shows a map of the relationship among the Ni content, Ni valence state, and diffusion coefficient in the NMC system at SOC = 1/3.

The D_s variation trend for the Ni rich group is related to not only the Ni content and Ni valence states but also the strain effect (related Li slab space). There is no Ni^{2+} state for both SOC = 1/3 and 1/2, and the Ni^{3+} content only increases little with the increasing Ni content (Table S2). By contrast, the Li slab space changes with the increasing Ni content significantly (e.g., from 2.612 to 2.701 Å with NMC from (532) to (622), Table S3). As the activation barrier is sensitive to the Li slab space, the strain effect cannot be neglected. Take the case of D_s from (532) to (622) as an example. The amounts of Ni^{3+} are the same for both of them at both SOC = 0.33 and SOC = 0.5 (Table S2), but the D_s for (622) is much larger. This can be attributed to the larger Li slab space of (622) with 2.701 Å, which is larger than that of (532) by 0.09 Å. Similarly, the decrease of the Li slab space from 2.701 Å in (622) to 2.553 Å in (71515) accounts for the drop of D_s from (622) to (71515), even though the Ni^{3+} content in (71515) is higher than that in (622) at SOC = 1/3 (Table S2). When Ni becomes the majority among the transition metal atoms, the Li slab space is more sensitive to the Ni content. As for the Ni-rich group, there are two factors that affect the Li slab space. On one hand, with the increasing Ni content, smaller Mn^{4+} and Co^{3+} are replaced by larger Ni^{3+} (Table S4), resulting in a larger transition slab space and smaller Li slab space. On the other hand, the reduced content of Mn^{4+} causes some amount of larger Ni^{2+} to be transformed to smaller Ni^{3+} and makes the Li slab space larger. These two mechanisms compete with each other, leading to the Li slab space first increasing from (532) to (622) and then decreasing from (622) to $LiNiO_2$ along the Ni-rich route. This is further validated by the less significant drop from (622) to (71515) at SOC = 0.5 compared with that at SOC = 0.33 (Figure 4). The ratio of Ni^{3+}/Ni^{4+} in (71515) is 0.52/0.18 at SOC = 0.33, while it is 0.35/0.35 at SOC = 0.5. When more Ni ions are oxidized to Ni^{4+} at a high SOC, Ni ions become smaller and the replacement of Mn/Co with Ni cannot significantly enlarge the transition metal space, leading to the smaller space change along (622)−(71515)−(811).

DOI: 10.1021/jacs.5b04040
J. Am. Chem. Soc. XXXX, XXX, XXX−XXX

The contents of Mn and Co play a correlated synergistic effect in the transition metal slab to tune the Li diffusion. The increased content of Mn^{4+} pushes the valence state of some Ni atoms from Ni^{3+} to Ni^{2+} to induce more advantageous Li-ion migration paths. The invariant Mn^{4+} also protects the NMC crystal structure free from either a spinel-like phase transition or any Jahn−Teller distortion of Mn^{3+}, thus ensuring the stability of the transition metal slab and the ordered Li-ion diffusion. The content of Mn^{4+} can affect the size of the transition metal slab through their smaller ionic radius and by controlling the ratio of Ni^{2+}/Ni^{3+}. The content of Co^{3+} not only affects the size of the transition metal slab through their smaller ionic radius but also can stabilize the Ni^{2+} in the transition metal layer. Due to the similar size of Ni^{2+} and Li^{+}, Ni^{2+} is more favorably located at Li 3b sites in the Li slab than Ni^{3+}. When such Ni^{2+} in the Li slab is oxidized to Ni^{3+} during delithiation, the NiO_6 octahedron in the Li slab would shrink to reduce the local Li slab space, which would increase the E_{eff} of Li-ion diffusion. This cation disorder effect is significant in the NCM materials with high Ni^{2+} content.[12] For example, $LiNi_{0.5}Mn_{0.5}O_2$ should have a high rate capability (fast Li diffusion), because half of the Li-ion activated states are contacted with Ni^{2+}. However, the high battery capacity (200 $mAh{\cdot}g^{-1}$) of $LiNi_{0.5}Mn_{0.5}O_2$ is achieved only at very low charge/discharge rates, which is attributed to the heavy cation disorder (nearly 8%−10%). Previous studies reported that Co doping of $LiNi_{0.5}Mn_{0.5}O_2$ could suppress the cation disorder effectively,[7,13] because the small size of low spin trivalent Co^{3+} (Table S4) decreases the transition metal slab and enhances the ligand field to stabilize the Ni^{2+} in the transition metal slab.

In summary, we investigate the kinetics of Li-ion diffusion vs selection of advantageous paths, and their effective diffusion barriers depended on activation energies and Li-slab space in NMC materials systematically. We then clarified how these factors tune the kinetics of Li diffusion in a delithiation process and for different NMC materials at the same delithiation state. Finally, because the "Ni = Mn" group can realize fast Li-ion diffusivity and high reversible capacity as the Ni-rich group and considering that low nickel material can be more stable than nickel-rich materials,[3c] we propose that the "Ni = Mn" group is a most promising way to design new NMC materials with high performance. This study can give some clues to how to design and further improve the performance of the layered cathode materials.

■ ASSOCIATED CONTENT

Supporting Information

Supporting Information provides details about first-principle calculation, models in kinetic study, experimental methods, tables of relevant lattice parameters and ionic radius, GITT results, Arrhenius linear fitting to obtain D_s at rt and a map of Ni content vs D_s, and suggestions about the recent hot Li_2MnO_3-based oxides. The Supporting Information is available free of charge on the ACS Publications website at DOI: 10.1021/jacs.5b04040.

■ AUTHOR INFORMATION

Corresponding Author

*panfeng@pkusz.edu.cn

Author Contributions

#Y.W., J.Z., and S.C. contributed equally.

Notes

The authors declare no competing financial interest.

■ ACKNOWLEDGMENTS

The work was financially supported by National Project for EV Batteries (20121110, OptimumNano, Shenzhen), Guangdong Innovation Team Project (No. 2013N080), Shenzhen Science and Technology Research Grant (Nos. ZDSY20130331145131323, CXZZ20120829172325895, JCYJ20120614150338154, JCYJ20130329181509637, and JCYJ20140417144423201), and the National Natural Science Foundation of China (No. 51302007).

■ REFERENCES

(1) (a) Tarascon, J. M.; Armand, M. *Nature* **2001**, *414*, 359−367. (b) Armand, M.; Tarascon, J.-M. *Nature* **2008**, *451*, 652−657. (c) Liang, Y. L.; Zhang, P.; Yang, S. Q.; Tao, Z. L.; Chen, J. *Adv. Ener. Mater.* **2013**, *3*, 600−605.

(2) Kang, K.; Meng, Y. S.; Bréger, J.; Grey, C. P.; Ceder, G. *Science* **2006**, *311*, 977−980.

(3) (a) Whittingham, M. S. *Chem. Rev.* **2004**, *104*, 4271−4302. (b) Goodenough, J. B.; Kim, Y. *Chem. Mater.* **2009**, *22*, 587−603. (c) Noh, H. J.; Youn, S.; Yoon, C. S.; Sun, Y. K. *J. Power Sources* **2013**, *233*, 121−130.

(4) (a) Ohzuku, T.; Makimura, Y. *Chem. Lett.* **2001**, *30*, 642−643. (b) Li, Z.; Chernova, N. A.; Roppolo, M.; Upreti, S.; Petersburg, C.; Alamgir, F. M.; Whittingham, M. S. *J. Electrochem. Soc.* **2011**, *158*, A516−A522. (c) Shaju, K.; Subba Rao, G.; Chowdari, B. *Electrochim. Acta* **2002**, *48*, 145−151.

(5) (a) Ren, H.; Huang, Y.; Wang, Y.; Li, Z.; Cai, P.; Peng, Z.; Zhou, Y. *Mater. Chem. Phys.* **2009**, *117*, 41−45. (b) Hwang, B. J.; Santhanam, R.; Chen, C. H. *J. Power Sources* **2003**, *114*, 244−252. (c) Guo, J.; Jiao, L. F.; Yuan, H. T.; Li, H. X.; Zhang, M.; Wang, Y. M. *Electrochim. Acta* **2006**, *51*, 3731−3735.

(6) Yamada, A.; Tanaka, M.; Tanaka, K.; Sekai, K. *J. Power Sources* **1999**, *81*−*82*, 73−78.

(7) Ellis, B. L.; Lee, K. T.; Nazar, L. F. *Chem. Mater.* **2010**, *22*, 691−714.

(8) (a) Yoon, W. S.; Grey, C. P.; Balasubramanian, M.; Yang, X. Q.; McBreen, J. *Chem. Mater.* **2003**, *15*, 3161−3169. (b) Li, D. C.; Sasaki, Y.; Kobayakawa, K.; Sato, Y. *Electrochim. Acta* **2006**, *51*, 3809−3813. (c) Li, D. C.; Sasaki, Y.; Kageyama, M.; Kobayakawa, K.; Sato, Y. *J. Power Sources* **2005**, *148*, 85−89. (d) Tran, N.; Croguennec, L.; Jordy, C.; Biensan, P.; Delmas, C. *Solid State Ionics* **2005**, *176*, 1539−1547.

(9) (a) Henkelman, G.; Jónsson, H. *J. Chem. Phys.* **2000**, *113*, 9978−9985. (b) Henkelman, G.; Uberuaga, B. P.; Jónsson, H. *J. Chem. Phys.* **2000**, *113*, 9901−9904.

(10) Van der Ven, A.; Ceder, G. *Electrochem. Solid State Lett.* **2000**, *3*, 301−304.

(11) Kang, K.; Ceder, G. *Phys. Rev. B* **2006**, *74*, 094105.

(12) Gu, M.; Belharouak, I.; Genc, A.; Wang, Z.; Wang, D.; Amine, K.; Gao, F.; Zhou, G.; Thevuthasan, S.; Baer, D. R.; Zhang, J.-G.; Browning, N. D.; Liu, J.; Wang, C. *Nano Lett.* **2012**, *12*, 5186−5191.

(13) (a) Saadoune, I.; Delmas, C. *J. Mater. Chem.* **1996**, *6*, 193−199. (b) Rougier, A.; Saadoune, I.; Gravereau, P.; Willmann, P.; Delmasa, C. *Solid State Ionics* **1996**, *90*, 83−90.

DOI: 10.1021/jacs.5b04040
J. Am. Chem. Soc. XXXX, XXX, XXX−XXX